Research Article

Determination of PV Generator *I-V/P-V* Characteristic Curves Using a DC-DC Converter Controlled by a Virtual Instrument

E. Durán,[1] J. M. Andújar,[1] J. M. Enrique,[1] and J. M. Pérez-Oria[2]

[1] *Department of Electronic, Computer Science and Automatic Engineering, University of Huelva, 21071 Huelva, Spain*
[2] *Technology and Automatic Systems Department, University of Cantabría, 39005 Santander, Spain*

Correspondence should be addressed to E. Durán, aranda@uhu.es

A versatile measurement system for systematic testing and measurement of the evolution of the *I-V* characteristic curves of photovoltaic panels or arrays (PV generators) is proposed in this paper. The measurement system uses a circuit solution based on DC-DC converters that involves several advantages relative to traditional methods: simple structure, scalability, fast response, and low cost. The measurement of the desired characteristics of PV generators includes high speed of response and high fidelity. The prototype system built is governed by a microcontroller, and experimental results prove the proposed measurement system useful. A virtual instrument (VI) was developed for full system control from a computer. The developed system enables monitoring the suitable operation of a PV generator in real time, since it allows comparing its actual curves with those provided by the manufacturer.

1. Introduction

The conversion efficiency of a solar cell is defined as the cell-produced power (W) divided by the input light irradiance (W/m^2) in standard test conditions (STC: 1000 W/m^2 and 25°C) and the surface area of the solar cell (m^2). Thus, conversion efficiency depends on many factors such as irradiation levels and temperature. Manufacture processes usually lead to differences in electrical parameters, even within the same type of cells. Moreover, if losses due to cell connections in a module are taken into account, it is difficult to find two identical PV modules.

On the other hand, the parameters provided by manufacturers of PV modules are measured in STC. However, such conditions rarely occur in field. Therefore, the estimate of the electrical characteristics of a module or array requires transferring these features to outdoor conditions, whose behavior cannot be predicted reliably in actual operation (i.e., the actual production of the PV facility).

Finally, measured by comparison over time, the real temporal degradation of the modules of a PV facility allows real production forecast and even manufactures claims for excessive uncovered damage.

In view of the foregoing, only the experimental measurement of the *I-V* and *P-V* curves allows us to get to know with precision the electrical parameters of a photovoltaic cell, module, or array. This measure provides very relevant information for the design, installation, and maintenance of PV systems [1, 2]. The experimental measurement of the *I-V* characteristic is of great importance, as it can be considered as a quality and performance certificate of every PV generator [3, 4].

The main points of the *I-V* and *P-V* curves characteristics are the short-circuit current (I_{sc}) or the maximum current at zero voltage, and the open-circuit voltage (V_{oc}) or the maximum voltage at zero current. For each point in the *I-V* curve, the product of the current and voltage represents the output power for that operating condition. The MPP produced by the PV generator is reached at a point on the characteristic where the product *I-V* is maximum (P_m in Figure 1(b)). The fill factor (FF) is defined as the ratio between P_m and the product $I_{sc} \cdot V_{oc}$, which shows curve squareness. Hence, $P_m = I_{sc} \cdot V_{oc} \cdot FF$: the closer to the unit the fill factor is, the better cell quality will be. Typical characteristic curves of a PV module are plotted in Figure 1, with irradiance and temperature as parameters.
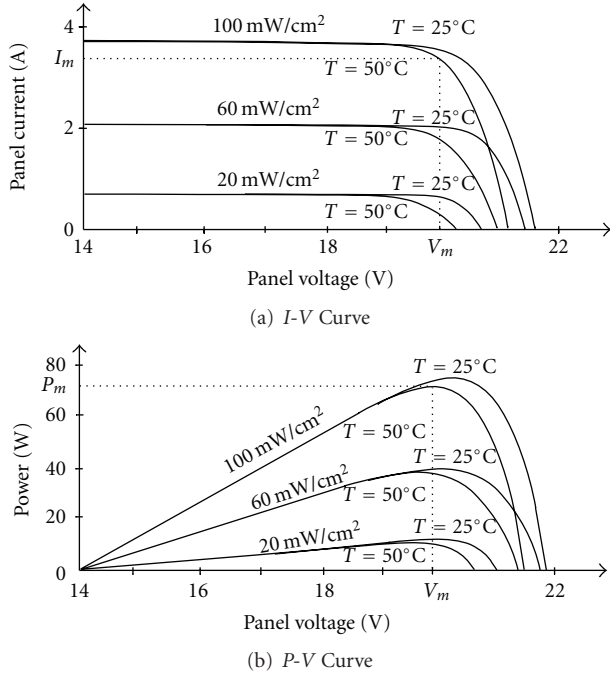
(a) *I-V* Curve

(b) *P-V* Curve

FIGURE 1: Characteristic curves of a PV module.

The basic principle to measure the *I-V* curve of a PV generator is based on the control of the current supplied between the zero current point (V_{oc}) and the short circuit point (I_{sc}). Different methods are proposed for this: variable resistor, capacitive load, electronic load, bipolar power amplifier, and four quadrant power supply. However, the cost, volume of measurements, speed, repeatability, accuracy, and ease of use and maintenance of a test system are factors that must be taken into account. An extensive review of different methods for measuring *I-V* curves of PV generators can be found in [5]. The most commonly used methods shall be briefly discussed in this section.

The simplest way to measure the *I-V* curve of a PV generator is to use a variable resistor *R* [6]. The value of *R* will be varied in progressive steps from zero to infinity in order to capture the points of the *I-V* curve from short circuit to open circuit by measuring voltage and current in each step. This method is only applicable to low-power PV generators due to the rather limited availability of resistors for higher power.

The capacitive method [7] uses a capacitor as the load. As the charge of the capacitor is increased, current drops and voltage rises. When the charge is completed, the current supplied by the PV generator becomes zero, and the open-circuit condition is achieved. To obtain a reliable *I-V* curve with the capacitor method, high-quality capacitors (low equivalent series resistance) with small losses are required.

The electronic load method [8] uses a transistor (usually a MOSFET) as the load. The resistance between drain and source and the flow of the current supplied by the PV generator are modulated through the gate-source voltage. When this method is used to trace the *I-V* curve of the PV generator, the MOSFET must operate in its three operation modes

(cut-off, active, and ohmic region). As a result, most of the power delivered by the PV generator must be dissipated by the MOSFET, which limits its application to medium power.

The bipolar power amplifier method is based on a traditional class-B power amplifier that uses two BJTs transistors as the load, for forward and reverse current, respectively. The bipolar transistors must operate in their three operational modes (cut-off, active, and saturation region). Therefore, as in the electronic load method, most of the PV generator delivered power must be dissipated by the transistors, thus limiting their application to medium power.

A four-quadrant power supply [9] is used to simulate real-world load characteristics for testing and evaluation of DC power supplies and other sources with a DC output voltage such as fuel cell, PV generators, and batteries. These loads can also be used to emulate the load reflected on high-voltage DC bus in electric vehicles, hybrid electric vehicles, and fuel cell vehicles. A four-quadrant power supply can be seen as a power supply whose output can be varied by a reference input signal or programmed to sweep a specific range of values. These types of power supplies are intrinsically expensive. Furthermore, four-quadrant power supplies working over 1 kW are limitedly available, so this method is not applicable to measure an array of PV modules.

This work aims at contributing a new experimental method for *I-V* curve measurement. It uses a new circuit solution based on a controllable DC load implemented by a single-ended primary inductance converter (SEPIC) [10]. The property of DC-DC converters to emulate a variable resistance is used for this application [11]. When obtaining the *I-V* curve of a PV generator, the most important parameter is the reliability with which the different points in this curve are reproduced. Thus, DC-DC converter efficiency becomes a secondary parameter in the proposed methodology. However, the actual curve at the PV generator terminals can be easily obtained from a quality curve and known converter efficiency, which is immediate.

The control scheme of the developed system is implemented in a cost-effective microcontroller PIC16F877 that generates the PWM signal to set the converter switching frequency. A sweep of the duty cycle allows capturing the abovementioned curve. The PIC microcontroller also re-ceives the voltage and current samples generated at the output terminals of the PV module, using the internal 8-channel multiplexed 10-b A/D converter. These values are transferred to a computer through an RS-232 protocol. Finally, a virtual instrument (VI) was developed using NI LabVIEW software to enable overall system control from a computer.

This paper is organized as follows. Section 2 analyzes the capability of different topologies of DC-DC converters for acting as resistance emulators. Section 3 describes the proposed system as well as the measurement technique used for capturing the *I-V* and *P-V* curves of a PV generator. Moreover, the different advantages in terms of capture mode, representation mode, controllable parameters, portability and flexibility are shown. Section 4 is devoted to the experimental validation of the developed prototype. Experimental results validate the theoretical analysis. Section 5 includes a

comparison between traditional methods and the solution proposed in this paper. Finally, some conclusions are drawn in Section 6.

2. DC-DC Converters as Emulators of Variable Resistance

DC-DC converters can increase or decrease the magnitude of the DC voltage and/or invert its polarity. This is accomplished by means of the pulse width modulation (PWM) technique, usually by a constant frequency. The duty cycle (D) is the ratio between time of conduction (T_{ON}) and switching period (T_s). The three basic configurations of converters (Buck, Boost, and Buck-Boost-Derived) are similar to a DC transformer in both continuous and discontinuous conduction mode (CCM and DCM). The relationship of transformation in a DC transformer can be controlled electronically by changing the duty cycle of the converter within the range $[0, 1]$. Figure 2 shows the basic DC-DC converters and the representation of input resistance versus duty cycle for CCM. The relations between input resistance (R_i is the emulated resistance at the output terminals of the PV module), equivalent inductance (L_{eq}), and the load connected to the converter (R) can be obtained in both CCM and DCM. The following expressions were obtained assuming converters without losses and small switching ripple magnitudes when compared to their respective DC components.

2.1. Buck Converter (Figure 2(a)). The following is fulfilled in CCM:

$$V_o = V_g \frac{T_{ON}}{T_s} = V_g \cdot D, \qquad I_g = I_o \cdot D \qquad (1)$$

and in DCM:

$$V_o = \frac{2 \cdot V_g}{\left(1 + \sqrt{1 + \left(8 \cdot L_{eq}\right) / \left(R \cdot D^2 \cdot T_s\right)}\right)},$$

$$I_g = \frac{2 \cdot I_o}{\left(1 + \sqrt{1 + \left(8 \cdot L_{eq}\right) / \left(R \cdot D^2 \cdot T_s\right)}\right)}. \qquad (2)$$

Defining the effective resistance (R_i) as $R_i = V_g/I_g$, the following is obtained:

$$R_i(\text{CCM}) = \frac{V_g}{I_g} = \frac{R}{D^2},$$

$$R_i(\text{DCM}) = \frac{V_g}{I_g} = \frac{R}{4}\left(1 + \sqrt{1 + \frac{8 \cdot L_{eq}}{R \cdot D^2 \cdot T_s}}\right)^2, \qquad (3)$$

where $L_{eq} = L$ for the Buck (single inductor) converter. Therefore, the value of resistance R_i (CCM) must be within the interval (Figure 2(g)), while the value of resistance R_i (DCM) must be within the range: $R_i \in [R/4 \cdot (1 + \sqrt{1 + 4K})^2, \infty)$, where $K = 2 L_{eq}/RT_s$.

This expression indicates that a Buck converter cannot emulate smaller resistances than the load and, therefore, does not reach values near the short-circuit current of the PV generator when used to obtain *I-V* curves.

2.2. Boost Converter (Figure 2(b)). The Following is Fulfilled in CCM:

$$V_o = \frac{V_g}{1 - D}, \qquad I_g = \frac{I_o}{1 - D} \qquad (4)$$

and in DCM:

$$V_o = \frac{V_g}{2}\left(1 + \sqrt{1 + \frac{2R \cdot D^2 \cdot T_s}{L_{eq}}}\right),$$

$$I_g = \frac{I_o}{2}\left(1 + \sqrt{1 + \frac{2R \cdot D^2 \cdot T_s}{L_{eq}}}\right). \qquad (5)$$

Now, the effective resistance (R_i) is given by

$$R_i(\text{CCM}) = R\,(1 - D)^2,$$

$$R_i(\text{DCM}) = \frac{V_g}{I_g} = \frac{4 \cdot R}{\left(1 + \sqrt{1 + (2 \cdot R \cdot D^2 \cdot T_s)/L_{eq}}\right)^2}, \qquad (6)$$

where $L_{eq} = L$ for the Boost (single inductor) converter.

In this case, R_i (CCM) $\in [0, R]$ (Figure 3(h)) and $R_i(\text{DCM}) \in [4 \cdot R/(1 + \sqrt{1 + 4/K})^2, R]$

This expression indicates that a Boost converter cannot emulate greater resistances than the load and, therefore, does not reach values near the open-circuit voltage of the PV generator.

2.3. Buck-Boost-Derived Converters (Figures 2(c)–2(f)). The following is fulfilled in CCM:

$$V_o = \left|V_g\right| \frac{D}{1 - D}, \qquad I_g = I_o \frac{D}{1 - D} \qquad (7)$$

and in DCM:

$$V_o = D \cdot \left|V_g\right| \sqrt{\frac{R \cdot T}{2 \cdot L}}, \qquad I_g = D \cdot I_o \sqrt{\frac{R \cdot T}{2 \cdot L_{eq}}}. \qquad (8)$$

The effective resistance (R_i) is given by

$$R_i(\text{CCM}) = \frac{V_g}{I_g} = \frac{R \cdot (1 - D)^2}{D^2},$$

$$R_i(\text{DCM}) = \frac{V_g}{I_g} = \frac{2 \cdot L_{eq}}{D^2 \cdot T_s}, \qquad (9)$$

where $L_{eq} = L$ for the Buck-Boost single inductor converter.

In this case, $R_i(\text{CCM}) \in [0, \infty)$ (Figure 2(i)) and $R_i(\text{DCM}) \in [(2L_{eq})/T_s, \infty)$.

Therefore, these last configurations are capable of sweeping the whole *I-V* curve of a PV generator in CCM, from open-circuit voltage (V_{oc}) to short-circuit current (I_{sc}).

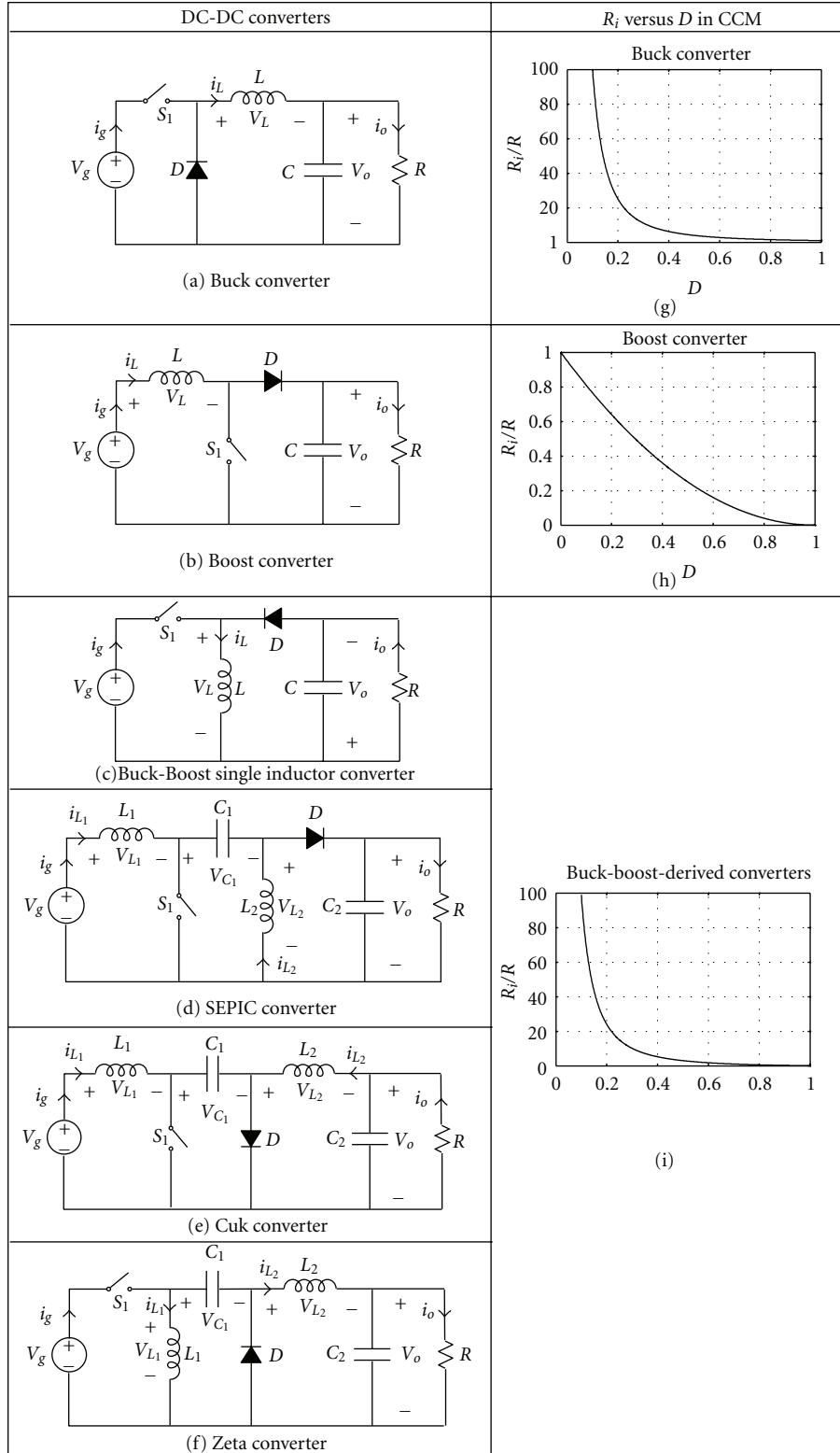| DC-DC converters	R_i versus D in CCM
(a) Buck converter	(g)
(b) Boost converter	(h)
(c)Buck-Boost single inductor converter	
(d) SEPIC converter	(i)
(e) Cuk converter	
(f) Zeta converter	

FIGURE 2: Different topologies of converters and representation of input resistance versus duty cycle for CCM.

The previous analyses of the Buck, Boost, and Buck-Boost-derived converters are summarized in Table 1. The dimensionless parameter K is a measure of the tendency of a converter to operate in DCM. Large values of K lead to CCM, while small ones lead to DCM. The critical value of K at the boundary between modes ($K_{\mathrm{crit.}}$) is a function of the duty cycle. If K is over the unit, then the converter operates in CCM for all duty cycles.

TABLE 1: Values of R_i, $R_{\text{crit.}}$, and $K_{\text{crit.}}$ for different DC-DC converters.

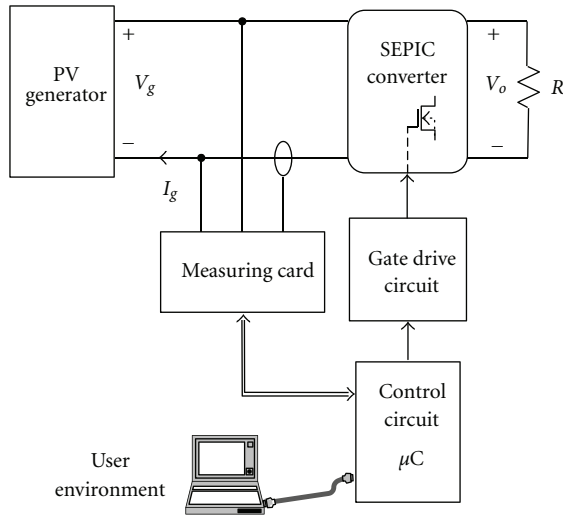|	Buck Converter	Boost Converter	Buck-Boost-derived Converters
R_i (CCM)	$\dfrac{R}{D^2}$	$R(1-D)^2$	$\dfrac{R\,(1-D)^2}{D^2}$
R_i (DCM)	$\dfrac{R}{4}\cdot\left(1+\sqrt{1+\dfrac{4K}{D^2}}\right)^2$	$\dfrac{4\cdot R}{(1+\sqrt{1+4D^2/K})^2}$	$\dfrac{K\cdot R}{D^2}$
$K_{\text{crit.}}$	$1-D$	$D(1-D)^2$	$(1-D)^2$
$R_{\text{crit.}}$	$\dfrac{2\,L_{\text{eq.}}}{(1-D)T_S}$	$\dfrac{2\,L_{\text{eq.}}}{D\,(1-D)^2\,T_S}$	$\dfrac{2\,L_{\text{eq.}}}{(1-D)^2\,T_S}$
With $K=\dfrac{2\,L_{\text{eq}}}{RT_S}$ and $\dfrac{1}{L_{\text{eq}}}=\dfrac{1}{L_1}+\dfrac{1}{L_2}$.		DCM occurs for $K<K_{\text{crit.}}$ or $R>R_{\text{crit.}}$	

FIGURE 3: Blocks diagram of the proposed system.

Considering previous discussion, it can be deduced that the only topologies that are capable of accomplishing the complete sweep of the *I-V* curve of the PV generators (i.e., from V_{oc} to I_{sc}) are those with Buck-Boost conversion ratio. Several topologies such as Buck-Boost (single inductor), Zeta, Cuk, and SEPIC provide the same conversion ratio and input resistance. Nevertheless, the input current in Buck-Boost and Zeta topologies is always discontinuous, because the switch is connected in series with the panel, thus causing significant harmonic components in the current and therefore producing high input ripple and significant noise problems. Cuk and SEPIC converters show nonpulsating input current. Therefore, *I-V* curve sweeping is carried out in a more reliable and less noisy manner. Consequently, these topologies are more suitable. Actually, both topologies present very similar characteristics: they use the same number of components, submit the switches to the same stress, and provide similar efficiency. From an analytical point of view, Cuk and SEPIC topologies are also similar. However, link capacitor (C_1) voltage must follow the input voltage for the SEPIC converter. This means that the capacitor size can be smaller, whereas, for the Cuk converter, it is the sum of the input and output voltage. Equations for both converters are identical.

3. System Overview

The block diagram of the proposed measurement system is shown in Figure 3. It mainly consists of a SEPIC DC-DC converter implemented with power MOSFETs, a low-cost microcontroller (μC), a measuring board with voltage and current sensors, and a gate-driver circuit. In general terms, the system operates as follows: the SEPIC converter emulates a resistor whose value is modified through the duty cycle of the PWM signal. This control signal is generated by the microcontroller, but its levels need to be adapted by a circuit to drive the switch transistor of the converter. Power MOSFETs (unlike bipolar transistors) have a considerable gate capacitance that must be charged beyond the threshold voltage. The gate-driver circuit provides a high output current to charge this gate capacitance within the time required. A measurement card formed by two Hall-effect sensors captures the values of current and voltage generated by the PV generator. This type of sensor was chosen because it needs no connection, is cheap, accurate, fast, and noise-immune, and has a wide bandwidth. Measurement with nonisolated current sensors affects the reproduction of values close to the short-circuit current (I_{sc}). In the same way, measurement with nonisolated voltage sensors affects the reproduction of values near V_{oc}. The analog values captured by sensors are scaled and applied to an internal 8-channel multiplexed 10-b A/D converter of the microcontroller and transferred to a computer via an RS-232 serial port. A virtual instrument (VI), developed using NI LabVIEW software and shown in Figure 4, allows processing and graphic representation of the mentioned voltage and current values. Moreover, the user can control all system parameters from the computer.

3.1. Operating Modes. The VI in Figure 4 was designed to facilitate system configuration. Control parameters were grouped and framed according to their purpose: operating modes, communication via serial port, PWM signal configuration, capture of information, and graphic representation. The system presents two operating modes denoted as "Tracer" and "Generator."

Tracer Mode. This is the main operating mode, since it allows all the required functions. The control block governed by the microcontroller generates the PWM signal whose main

parameters (frequency, duty cycle, and sweep time) can be adjusted by the user from the front panel. This signal is applied through a driver circuit to the DC-DC converter. Next, the levels of current and voltage generated by the PV generator are captured by Hall-effect sensors, processed by the microcontroller, and transferred to the computer via the serial port. Then, this information is graphically depicted in the user environment showing the *I-V* and *P-V* curves. The number of captured samples of voltage and current can also be fixed by the user.

Generator Mode. It constitutes an alternative operating mode where the user configures the parameters of the PWM signal that is generated by the microcontroller and applied to the converter. Unlike the "Tracer Mode," the levels of current and voltage generated by the PV generator are not captured by Hall-effect sensors and are not therefore sent to computer for graphic representation. Its main utility is that it allows the system to continue performing without the measuring card depicted in the block diagram in Figure 3. In this case, *I-V* curves could be captured and evaluated for direct display with another measurement system or equipment (e.g., an oscilloscope equipped with a current probe).

3.2. Additional Properties. The PWM signal is generated with the Capture/Compare/PWM (CCP) modules of the microcontroller. Each module has a 16-bit register that must be configured. The PWM period is specified by writing to the P_{R2} register and is given by.

$$\text{PWM Period} = [(P_{R2}) + 1]4T_{\text{OSC}}(\text{TMR2 Prescale Timer}). \tag{10}$$

"TMR2 Prescale Timer" can be set at 1, 4, or 16. T_{OSC} is the microcontroller clock period ($F_{\text{OSC}} = 20\,\text{MHz}$). Therefore, the PWM frequency can be adjusted between 1.22 kHz (for $P_{R2} = 0$ and Prescale Timer = 1) and 5 MHz (for $P_{R2} = 255$ and Prescale Timer = 16). Next, the fixed PWM duty cycle (D) is specified by writing to the CCPR1L register and two bits of CCP1CON⟨5 : 4⟩ register as

$$\text{PWM Duty Cycle} = (\text{CCPR1L} : \text{CCP1CON}\langle 5 : 4\rangle)$$
$$\cdot T_{\text{OSC}} \cdot (\text{TMR2 Prescale Timer}). \tag{11}$$

The microcontroller firmware was developed using C compiler from Microchip.

The VI allows configuring the PWM signal from the computer as follows: first, the user sets a switching frequency (from 1.22 up to 5 MHz) and a duty cycle between 0 and 1. Moreover, the user can set the duty cycle sweep (DCS) and sweep time. When a DCS between 0% and 100% is chosen, the time of conduction T_{ON} increases from 0 to 1 at regular time intervals, and when T_{ON} is equal to the switching period (T_s), $T_{\text{ON}} = T_s$, DCS starts to decrease. This process continues cyclically. These regular time intervals can also be set by the user. The sweep up and down presents the advantage that the *I-V* curve of the solar panel can be

TABLE 2: Electrical characteristics of the Isofoton I-94/12 module.

Open-circuit voltage	$V_{\text{oc}} = 19.8\,\text{V}$
Short-circuit current	$I_{\text{sc}} = 6.54\,\text{A}$
Maximum power	$P_m = 94\,\text{W}$
Max. current at MPP	$I_m = 5.88\,\text{A}$
Max. voltage at MPP	$V_m = 16\,\text{V}$

drawn in both directions: from the open-circuit voltage (V_{oc}) to short-circuit current (I_{sc}) and vice versa. This will allow studying the hysteresis effect due to capacitive effects. A novel characteristic of this system is that the DCS can be configured for values different from 0 and 1 (e.g., a duty cycle sweep for D between 0.3 and 0.8). The advantage is that the *I-V* curve can be depicted by zones, or even an only point of the curve (e.g., D from 0.41 to 0.42) can be depicted.

The sweep period (T_{SWEEP}) can be obtained by the expression:

$$T_{\text{SWEEP}} = \frac{T_s}{4\,T_{\text{OSC}}}\Big[t_{\text{Delay}} + T_s\Big], \tag{12}$$

where T_{OSC} is the clock period for the microcontroller ($F_{\text{OSC}} = 20\,\text{MHz}$), T_S is the switching period, t_{Delay} is the regular time interval chosen, and T_{SWEEP} is the time of sweep obtained. For example, this equation establishes a T_{SWEEP} of 208 ms, with a delay time (t_{Delay}) of 1 ms and 200 steps for a DCS between 0% and 100%. For a DCS between 0% and 50%, half of the time is taken (104 ms) to cover twice the previous frequency. Note that if delay time is zero, DCS time would then be only 8 ms (each step or increase of T_{ON} is realized every 40 μs), which is a too fast time to be represented by many measurement systems. A complete description of the microcontroller-based DCS to obtain the *I-V* curve of PV modules can be found in [12].

Finally, the developed measurement system presents other properties such as its capacity for processing the large number of captured points by implementing a polynomial approximation with NI LabVIEW software (see curves in Figure 4). Additional information on V_{oc}, I_{sc}, maximum power point (MPP), and fill factor (FF) is also provided by the VI, as shown in Figure 4.

4. Experimental Results

For experimental measurements, a SEPIC converter was connected to an Isofoton I-94/12 module with the electrical characteristics reported in Table 2. These measurements were completed in standard conditions (irradiance 1000 W/m^2 and 25°C cell temperature).

Figure 5 shows the laboratory experimental prototype developed to obtain the results described in this paper, where a vertical implementation was chosen. The prototype was developed to measure *I-V* curves of PV modules of similar electrical characteristics to I-94/12 (the scaling of the system developed for higher power is immediate, since its architecture and mode of operation remain unchanged). For selection of the link capacitor C_1 in a conventional SEPIC converter, it is assumed that voltage in this capacitor
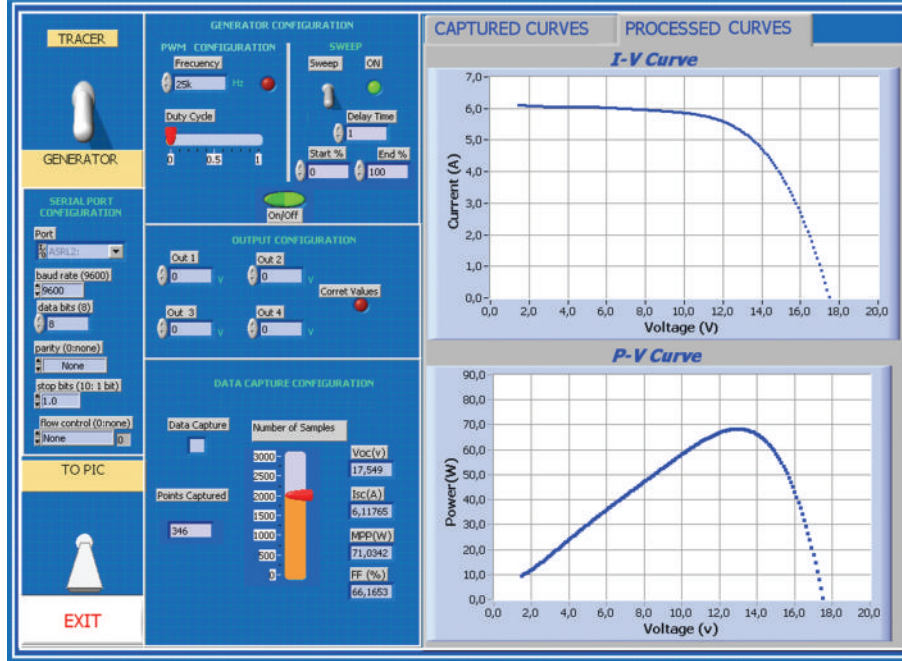
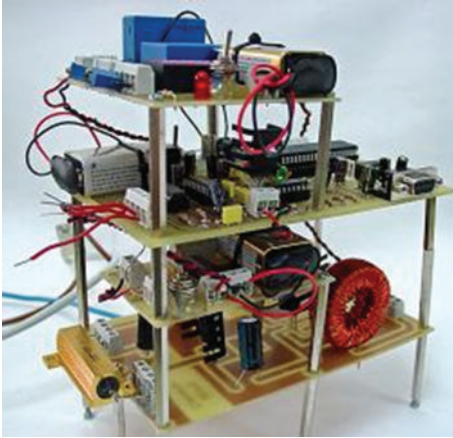FIGURE 4: Virtual instrument based on LabVIEW interface.

FIGURE 5: PCBs of the prototype.

must be constant. When the prototype operates as a tracker of PV curve, the capacitor voltage is under the following two conflicting constrains: (1) presenting a nearly constant value within a switching period and (2) following the input voltage in the sweep period of the I-V curve of the PV generator (sweep frequency, ω_{SWEEP}). Therefore, the resonant frequency (ω_r) of C_1, L_1, and L_2 must be greater than the sweep frequency to avoid input current oscillations. Besides, ω_r must be lower than the switching frequency (ω_S) to assure almost constant voltage, and the resonant frequency must be such that the converter operation mode is neither DQRM (discontinuous quasiresonant mode) nor DCVM (discontinuous-capacitor-voltage mode), that is

$$\omega_S > \omega_r > \omega_{\text{SWEEP}}, \quad \text{with}$$

$$\omega_r^2 = \frac{1}{C_1(L_1 + L_2)}, \qquad C_1 > \frac{D^2 \, T_s}{2 \, R}. \tag{13}$$

If $f_S = 100 \, f_r$ and $f_r = 10 \, f_{\text{SWEEP}}$ are chosen, with a switching period (T_s) of 40 μs, then the previous inequalities are satisfied for $C_1 = 470 \, \mu$F.

The selection of the inductors L_1 and L_2 is made using the desired ripple value of the input current. Its peak-to-peak value is given as

$$\Delta i_{L_1} = \frac{V_g}{L_1} D T_s. \tag{14}$$

Its maximum value occurs for $D = 1$ and $V_g = V_{\text{oc}}$. Therefore, L_1 can be obtained considering the specified maximum current ripple. The value of Δi_{L_1} is commonly a percentage of the value of average input current. It is undesirable to allow Δi_{L_1} to become too large, as it would increase the peak currents of the inductor and semiconductor switching devices, thus increasing their size and cost. We have considered $L_{\text{eq}} = 160 \, \mu$H and $L_1 = 800 \, \mu$H, which provides a smaller maximum ripple than I_{sc} with $L_2 = 200 \, \mu$H.

The selection of the load resistance R is realized to operate in CCM. The following inequalities must be held (see Table 1):

$$K > K_{\text{crit.}} \implies \frac{2 \, L_{\text{eq}}}{R T_s} > (1 - D)^2. \tag{15}$$

The previous must also be fulfilled for $D = 0$:

$$\frac{2 \, L_{\text{eq}}}{T_s} > R. \tag{16}$$

Selecting a switching period (T_s) of 40 μs, the above inequality is satisfied for $R = 5 \, \Omega$.

The power dissipated by load resistance R can be evaluated considering that it is equal to that produced for the

TABLE 3: Electrical characteristics of the components used for the SEPIC Converter.

Schottky Diode	MBR 1045	45 V, 10 A, 0.45 V at 6 A, 100°C
MOSFET	MTP 15N06VL	60 V, 15 A, 85 mΩ
L_1	CH 820088	820 μH, 8.8 A, 110 mΩ
L_2	CH 220086	220 μH, 8.6 A, 42 mΩ
C_1	TK series	470 μF, 25 V
C_2	TK Series	330 μF, 25 V
R	ARCOL	4.7 Ω, 25 W

TABLE 4: Electrical characteristics of the components used in the control circuit board and the measuring card.

μController	PIC 16F877	40-Pin 8-Bit CMOS Flash
Communication series	MAX 232	Multichannel RS-232, Driver/Receiver
Current sensor	LEM-LA 55-P/SP1	Closed Loop Hall Effect Current Sensor
Voltage sensor	LEM-LV 25-P	Closed Loop Hall Effect Voltage Sensor
Operational amplifier	OP-270	Monolithic Dual OPAM
Isolated 3 W dual output	TEL 3–1222	DC-DC Converter, DIL-24 Plastic Package

PV generator during the sweep time (assuming converters without losses). The voltage and the current at the PV generator terminals make a transition between V_{oc} and I_{sc} points. The current shows a rise time (the voltage falls) approximately equal to the sweep period (T_{SWEEP}) and can be integrated to find the power dissipated by load resistance R. The average power of the load resistance R can be obtained by means of the following general equation:

$$P_R = \frac{V_{\text{oc}} \, I_{\text{sc}}}{a} \frac{t_{\text{rise}}}{T_{\text{SWEEP}}}, \qquad (17)$$

where t_{rise} is the rise time of the current (fall time of the voltage) and a can be defined as a transition parameter: For linear transition $a = 6$ and for rectangular transition $a = 2$.

Considering $t_{\text{rise}} \approx T_{\text{SWEEP}}$, $a = 5$, $V_{\text{oc}} = 19.8$ V, and $I_{\text{sc}} = 6.54$ A, the average power dissipated by load resistance R is approximately 25 W.

The standard components used in the implementation of the SEPIC converter are summarized in Table 3.

Table 4 shows the most important electrical parameters of the components used in the implementation of the control circuit and the measuring card, which includes the sensors and operational amplifiers used for signal conditioning.

To ensure appropriate performance of the proposed system when measuring the I-V and P-V characteristic of PV modules, a comparison is made between the measure provided by an oscilloscope and the one monitored with NI LabVIEW interface, for the same module and climatic conditions. Thus, a LeCroy 500 MHz oscilloscope was used for measuring the experimental results. Figure 6 shows the measures of voltage, current, and power at the PV module terminals (during two sweep cycles) provided by the aforementioned oscilloscope and the developed system. Experimental results are in good agreement in both measures, as it can be deduced from the results of the voltage-current products given in the oscilloscope screenshot. Good similarity is achieved between both measures. Similar results are achieved for the three main points: $V_{\text{oc}} = 17$ V, $I_{\text{sc}} = 6$ A, and $P_m = 71$ W, with FF = 66, in these conditions.

An additional property of the implemented system is its ability to reproduce a piecewise of these curves, as the control circuit allows configuring the duty cycle sweep (DCS) for values different from 0 and 1. Figure 7 shows a segment of the I-V curve for the PV module around V_{oc}, when DCS is performed from 0 to 50% of the duty cycle, for this DCS, half of the necessary time (approximately 104 ms) to cover

twice the frequency obtained in Figure 6 (208 ms). Note that, as in this zone of the curve, there is a little voltage variation, whereas the current shows great variation. In this zone, the PV module works like a voltage source. Figure 8 shows a piecewise of the I-V curve around I_{sc} and P_m when DCS is performed from 50 to 100%. The PV module characteristic is described just in the region where the maximum power point is placed in. In the I_{sc} zone, there is a little current variation, whereas the voltage shows great variation. In this zone, the PV module works like a current source.

5. Discussion

In order to emphasize the properties of the developed system, a general comparison of the most commonly used methods is provided. The comparison is carried out with the following fundamental parameters for measurement systems.

Flexibility. Flexibility is an important factor of comparison. The proposed method based on DC-DC converters allows configuring sweep speed and direction. By modifying the duty cycle, specific zones of the I-V curve can be partially examined. It can be operated continuously around the maximum power point of the photovoltaic module under test. With a four-quadrant power supply, a partial reproduction of the I-V curve is also possible, but requires a complex programming of the signal. The methods based on electronic load also show high flexibility, but the reproduction of points around the MPP requires excessive power dissipation, especially with high-power generators, since transistors operate in their linear zone. In the capacitive load method, the I-V curve reproduction is not cyclic, so a direct visualization or a partial reproduction of the I-V curve is not possible.

Modularity. Scalable and modular instrument configuration is also an important parameter for comparison purposes. The method based on DC-DC converters allows system expansion by just connecting DC-DC converters in parallel. In the development of new paralleling techniques for DC-DC converters, interleaved power conversion is one of the most promising recently reported alternatives. This technique consists of phase shifting the control signals
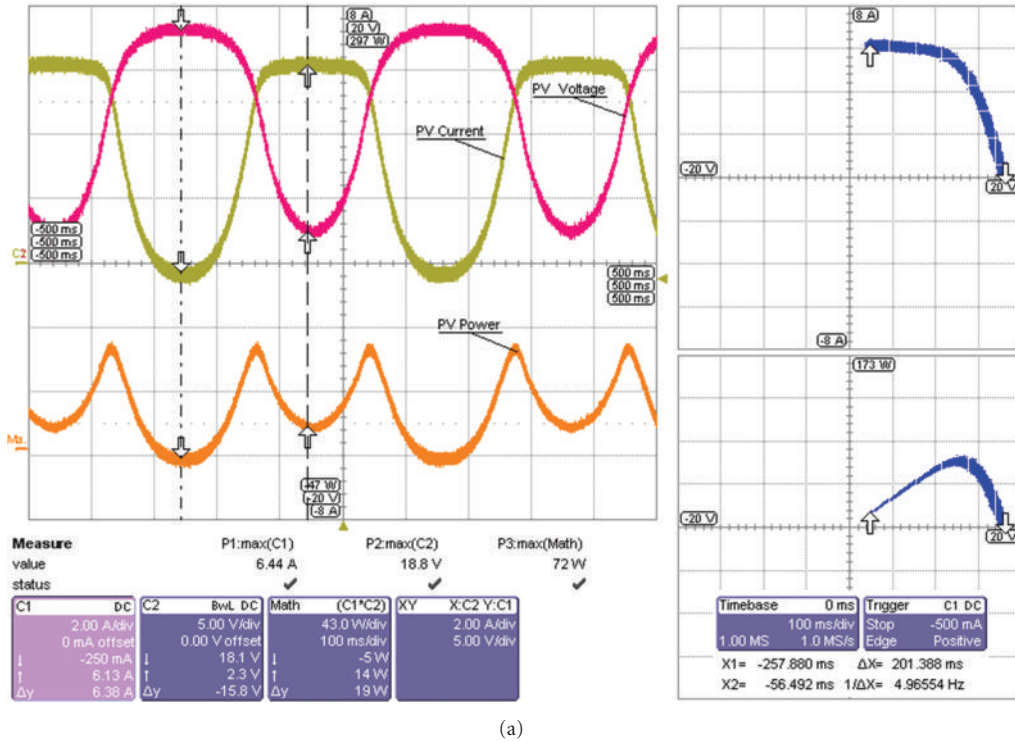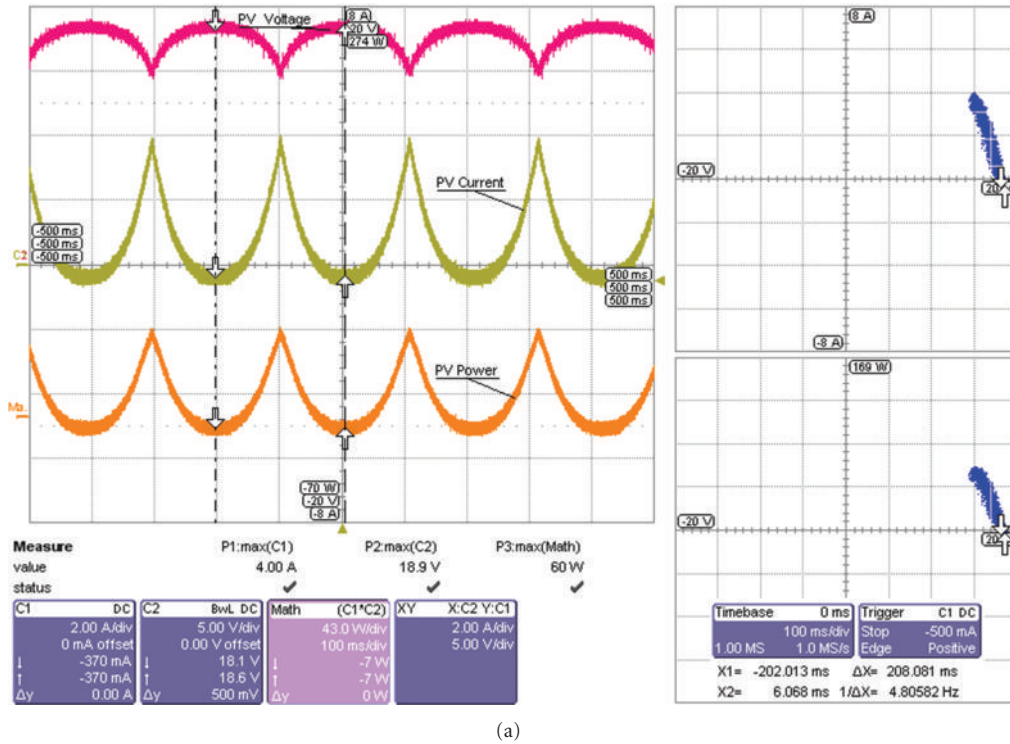
(a)
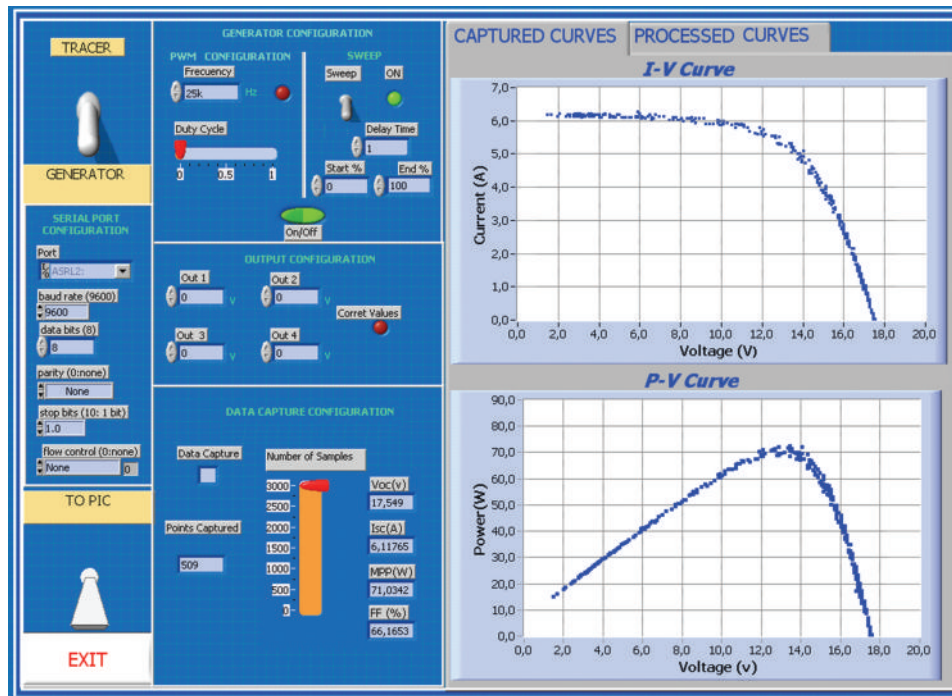
(b)

FIGURE 6: (a) Current (Channel C1: 2 A/div, 100 ms/div), voltage (Channel C2: 5 V/div, 100 ms/div), and power (Math C1*C2: 43 W/div, 100 ms/div) measurement. XY representation. (b) *I-V* and *P-V* curves obtained by means of the proposed system. DCS from 0 to 100%.

of several converters in parallel operation at the same switching frequency. As a result, the input current shows lower ripple amplitude. However, the interleaving technique requires increased circuit complexity (greater number of components and further auxiliary circuitry). In this case, a

microcontroller with several independent timers capable of generating the different PWM signals could be used.

Both the capacitive load and the electronic load methods involve difficulties when the power of the tested PV generator increases. The main design concerns are speed and power
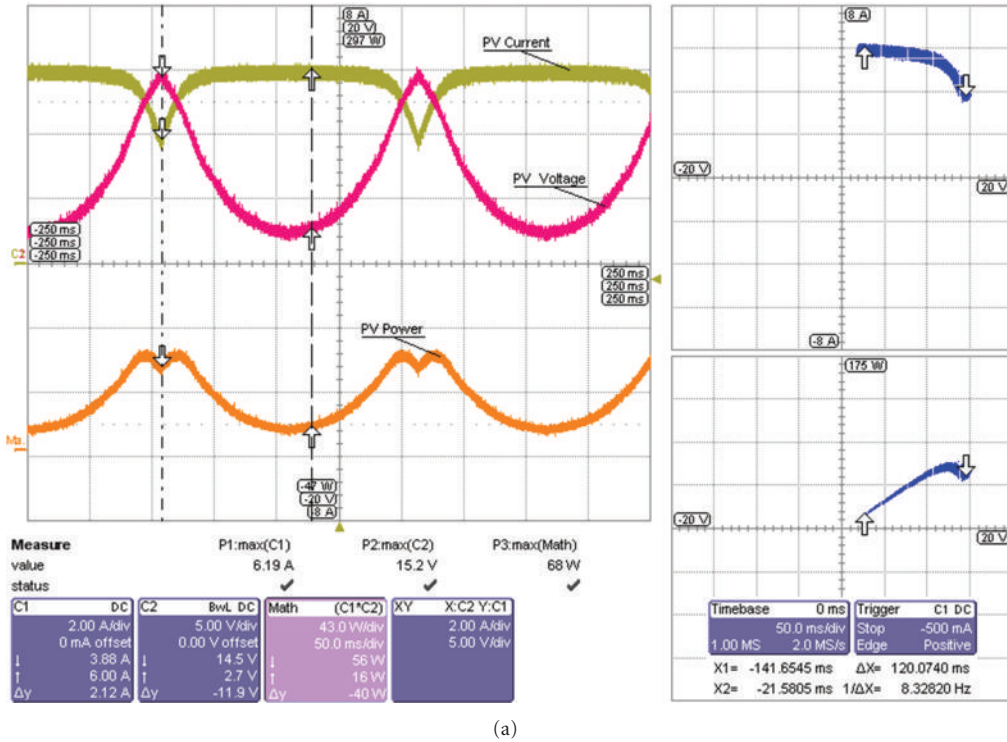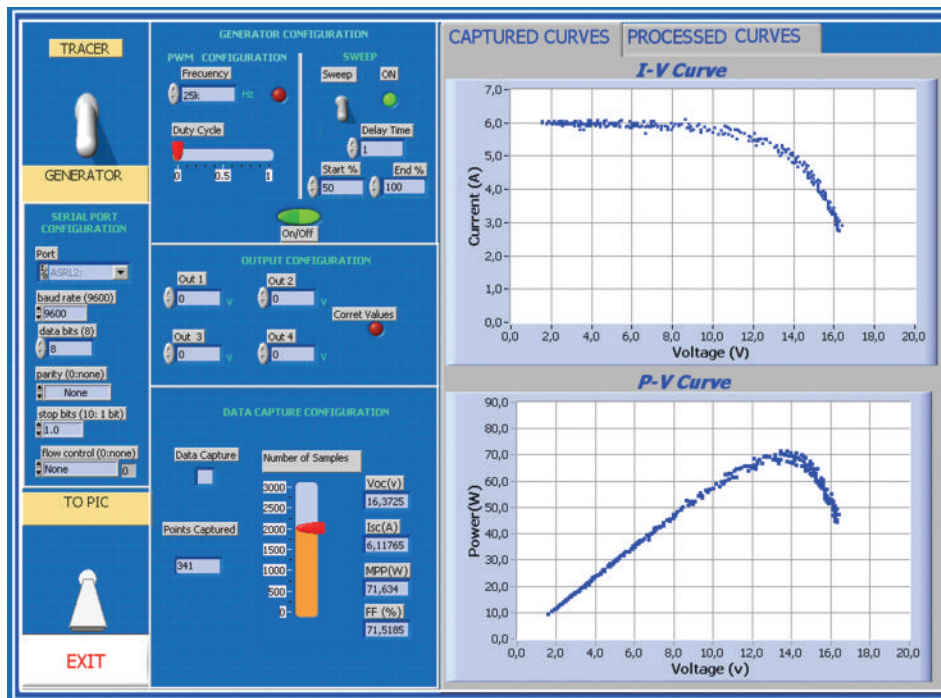
(a)
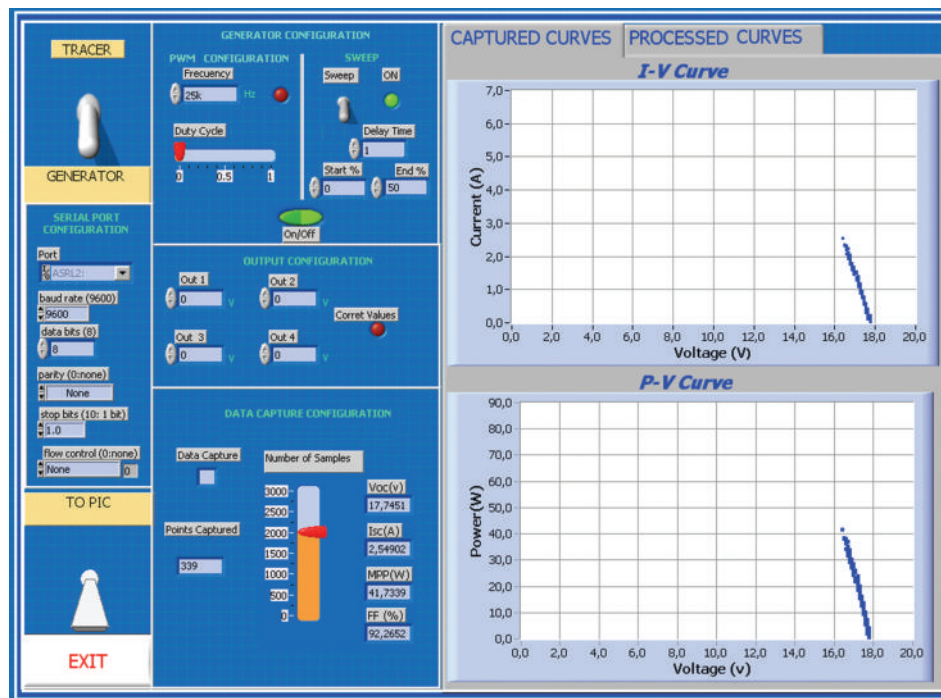
(b)

FIGURE 7: (a) Current (Channel C1: 2 A/div, 100 ms/div), voltage (Channel C2: 5 V/div, 100 ms/div), and power (Math C1*C2: 43 W/div, 100 ms/div) measurement. XY representation. (b) *I-V* and *P-V* curves obtained by means of the proposed system. DCS from 0 to 50%.

dissipation. In the case of a four-quadrant power supply, modularity is only possible with some manufacturers, providing a way to combine several supplies and allowing controlling them like a single supply, thus involving increased cost.

Fidelity. Method reliability is hard to evaluate because it largely depends on the data acquisition system. However, with the method based on DC-DC converters, high fidelity is achieved even for high speed sweeping. An exhaustive analysis of the reviewed methods reveals that it is difficult to

(a)

(b)

FIGURE 8: (a) Current (Channel C1: 2 A/div, 50 ms/div), voltage (Channel C2: 5 V/div, 50 ms/div), and power (Math C1*C2: 43 W/div, 50 ms/div) measurement. XY representation. (b) I-V and P-V curves obtained by means of the proposed system. DCS from 50 to 100%.

reproduce the exact point of zero voltage (I_{sc}). In the method based on DC-DC converters, it is due to the nonidealities of the components; moreover, it is less noticeable as short circuit current decreases. This proves that the effect presents a resistive feature mainly related to the MOSFET-associated resistance in conduction and to the inductance L_1-associated resistance. These nonidealities can also be observed not to excessively degrade the reproduction of the panel's I-V curve, mainly because—in the area where they appear—both the curve's slope and current variation are virtually null. In

TABLE 5: Comparison between different methods.

	Flexibility	Modularity	Fidelity	Fast Response	Direct Display	Cost
Variable resistor	Medium	Medium	Medium	Low	No	Low
Capacitive load	Low	Low	Medium	Low	No	High
Electronic load	High	High	Medium	Medium	Yes	High
Bipolar power amplifier	High	High	High	Medium	Yes	High
4-Quadrant power supply	Low	Low	High	High	No	High
DC-DC converter	High	High	High	High	Yes	Low

this area, the photovoltaic module can be compared to a constant current source of I_{sc} value, and so its effect can be considered irrelevant. This effect is significantly minimized by connecting several inductors and MOSFETs in parallel. The four-quadrant power supply method only needs an interpolation around zero volts. Interpolation can also be applied in the capacitor method, but only if a prior negative charge is imposed. With the variable resistor and the electronic load methods, extrapolation is necessary.

Fast Response. A fast response of operation is particularly interesting because it ensures that all points in the curve are obtained with the same climatic conditions. The highest requirements of operation speed for *I-V* measuring systems are necessary to measure accuracy both in laboratory (indoor) and field (outdoor). For the sake of accuracy, ambient conditions must not change significantly between the *I-V* curves traced. Besides, fast response of operation reduces overheating and the size of the components and the load. Both the four-quadrant power supply and DC-DC converters methods give a fast response of operation. Thus, the entire *I-V* curve can be determined within a few hundred milliseconds. In the capacitor method, the charging capacitor time is directly proportional to the value of the capacitor and the open-circuit voltage of the PV generator and indirectly proportional to the short-circuit current of the PV generator. Furthermore, the higher the speed of the measuring system is, the smaller the size of the required capacitor shall be. Nevertheless, the capacitor method requires discharging the capacitor before any further measurement; this extra time renders the capacitive method slower. The operation times of the capacitor method are usually below 1 s. In the electronic load methods, greater dispersion in measurement times is observed, depending of waveform at the terminals of gate or base for transistors (lineal ramp, sinusoidal, etc.) and also the type of control (with or without feedback). This means that the measuring time needed by some electronic loads is sometimes comparable to that reported in the four-quadrant power supply method and some others similar to that reported in the capacitor method.

Direct Display. It provides the opportunity for a quick first test of the module. However, not all methods allow direct display. The *I-V* curve reproduction is not cyclic in the variable resistor and capacitive load methods, and, therefore,

direct display or partial reproduction of the curve cannot be achieved.

Cost. Usually a good cost evaluation can be made by knowing the features of the data acquisition system, the analog or digital technique used, whether it requires software and programming, and the number of sensors. Eliminating current and voltage sensors leads to considerable cost reduction. The capacitive load method requires speed of acquisition and memory storage within the instrument, thus being costly. Perhaps the best way to evaluate all methods in terms of cost is taking into account all the previous features as a complete set. Thus, the method based on DC-DC converters is less expensive because it is flexible, modular, and reliable. Furthermore, it provides high-power density and allows direct display of the *I-V* curve.

Table 5 summarizes the properties of each method. Note that the method based on DC-DC converters shows features that make it preferable for the measurement of the *I-V* curve of photovoltaic modules. A drawback of DC-DC converters is the current ripple by the inductor due to the switching technique that does not exist in the classical methods. Nevertheless, some techniques developed to reduce the ripple include coupled inductors and interleaved DC-DC converters. Moreover, a DC-DC converter provides high power density, can be operated in parallel for higher power ratings, and can be easily reconfigured to obtain a wide variety of ratings.

6. Conclusions

A complete experimental system to monitor PV generators based on SEPIC converters is presented in this paper. A microcontroller generates the control signals for the DC-DC converter and receives the current and voltage samples of the solar panel. These samples are transferred via a serial port to a PC, where a virtual instrument was developed to control all system parameters. The prototype can measure the *I-V* characteristic curve of PV generators in both directions, from either short-circuit current I_{sc} to open-circuit voltage V_{oc} or from V_{oc} to I_{sc}, several times per second, which ensures that all points of the curve are obtained with the same climatic conditions. Experimental results agree with the theoretical analysis performed for the development of this methodology. The proposed method is compared to traditional ones. This

method is proven to offer new possibilities for measuring the *I-V* curve of a PV generator, as it is both quicker and cheaper than conventional methods.

Finally, knowledge of real curves of a module or array enables to get to know their actual production and, by comparing the curves over time, to assess their degree of degradation by weathering.

Acknowledgments

References

[1] N. Onat, "Recent developments in maximum power point tracking technologies for photovoltaic systems," *International Journal of Photoenergy*, vol. 2010, Article ID 245316, 11 pages, 2010.

[2] E. Durán, J. M. Andújar, J. Galán, and M. Sidrach-De-Cardona, "Methodology and experimental system for measuring and displaying I-V characteristic curves of PV facilities," *Progress in Photovoltaics: Research and Applications*, vol. 17, no. 8, pp. 574–586, 2009.

[3] M. M. Mahmoud, "Transient analysis of a PV power generator charging a capacitor for measurement of the I-V characteristics," *Renewable Energy*, vol. 31, no. 13, pp. 2198–2206, 2006.

[4] P. Sanchis, J. López, A. Ursúa, E. Gubía, and L. Marroyo, "On the testing, characterization, and evaluation of PV inverters and dynamic MPPT performance under real varying operating conditions," *Progress in Photovoltaics: Research and Applications*, vol. 15, no. 6, pp. 541–556, 2007.

[5] E. Durán, M. Piliougine, M. Sidrach-de-Cardona, J. Galán, and J. M. Andújar, "Different methods to obtain the I-V curve of PV modules: a review," in *Proceedings of the 33rd IEEE Photovoltaic Specialists Conference (PVSC '08)*, San Diego, Calif, USA, 2008.

[6] E. E. Van Dyk, A. R. Gxasheka, and E. L. Meyer, "Monitoring current-voltage characteristics and energy output of silicon photovoltaic modules," *Renewable Energy*, vol. 30, no. 3, pp. 399–411, 2005.

[7] J. Muñoz and E. Lorenzo, "Capacitive load based on IGBTs for on-site characterization of PV arrays," *Solar Energy*, vol. 80, no. 11, pp. 1489–1497, 2006.

[8] Y. Kuai and S. Yuvarajan, "An electronic load for testing photovoltaic panels," *Journal of Power Sources*, vol. 154, no. 1, pp. 308–313, 2006.

[9] M. G. Guvench, C. Gurcan, K. Durgin, and D. MacDonald, "Solar simulator and I-V measurement system for large area solar cell testing," in *Proceedings of the American Society for Engineering Education Annual Conference & Exposition*, pp. 12747–12753, 2004.

[10] E. Durán, F. Segura, J. Galán, and M. Sidrach-De-Cardona, "An approach to obtain the V-I characteristic of fuel cells by means of dc-dc converters," in *Proceedings of the 34th Annual Conference of the IEEE Industrial Electronics Society (IECON '08)*, pp. 2290–2295, November 2008.

[11] S. Singer, "The application of loss-free resistors in power processing circuits," *IEEE Transactions on Power Electronics*, vol. 6, no. 4, pp. 595–600, 1991.

[12] E. Durán, J. Galan, M. B. Ferrera, J. M. Andujar, and M. Sidrach-de-Cardona, "A new application of duty cycle sweep based on microcontroller to obtain the I-V characteristic n curve of photovoltaic modules," in *Proceedings of the IEEE International Conference on Industrial Technology (ICIT '08)*, pp. 1023–1028, April 2008.